Robex Seminar

Interval-based fault-detection of GNSS signal using land-based cameras for remote ship piloting operations

Morgan Louédec, Solène Boudot, Dimitrios Papageorgiou1 & Roberto Galeazzi

11th September 2025

Outline

Context - Remote pilotage in harbour environment

Tools - Interval analysis

Design of a Fault detection method with tubes

Experimental application

Results

Outline

SLGreen project

aprendio

DanPilot

MAERSK

Shipping Lab
Driving Future Maritime Technology

The Benefits ot remote pilotage

Remote piloting:

- **Increase safety**, by avoiding risky ladder boarding, which is the most common boarding method
- **Reduce fuel consumption**. Pilot's ships are not used. Cargo ships do not have to stop for boarding

Figure 1: DanPilot's ship

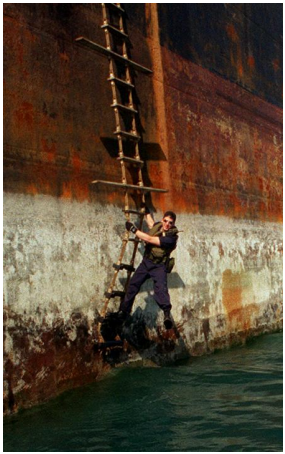

Figure 2: Ladder boarding

Perception & Communication, the challenges of remote pilotage

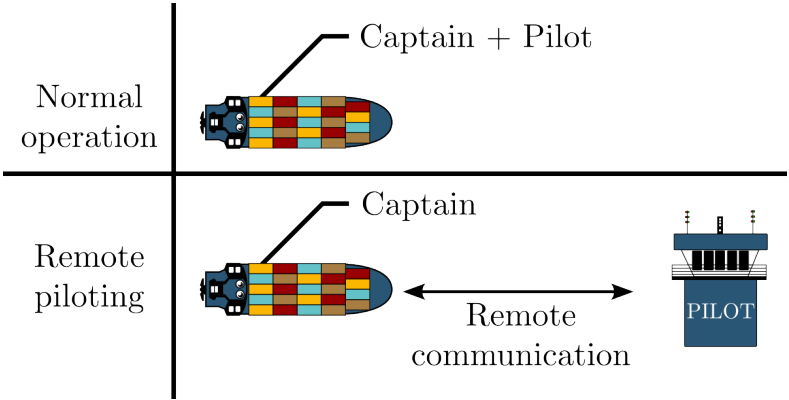

Remote pilot's perception relies on Maritime sensors

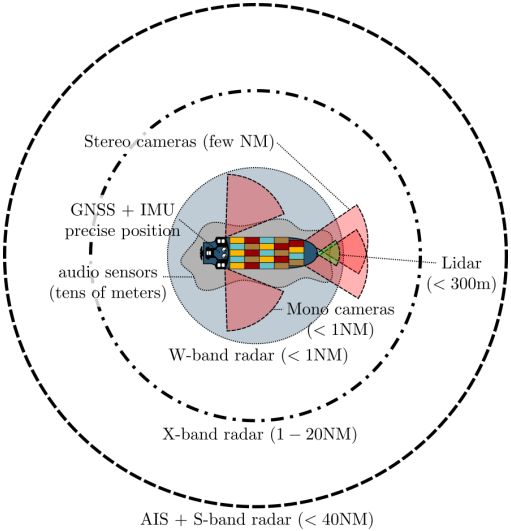

Large Data Visualization

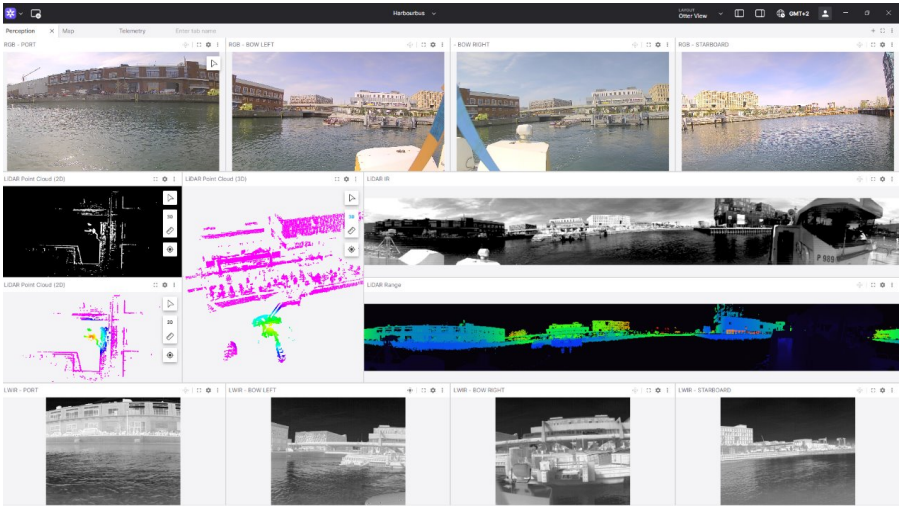

Problem – detecting falsification in the transmission during a docking manoeuvre using land-based sensors

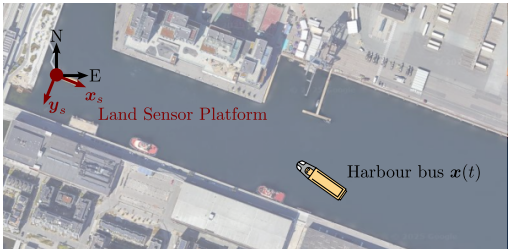

Figure 3: The ship docks near the Land Sensor Platform

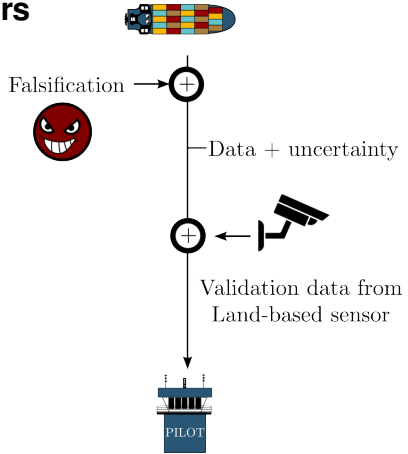

Figure 4: Data Flow

Outline

Tubes

A n-dimensional **tube** $[\boldsymbol{x}](\cdot) : \mathbb{R} \rightarrow \mathbb{IR}^n$ is a time dependent n-dimensional box. A trajectory $\boldsymbol{x}(\cdot)$ belongs to the tube $[\boldsymbol{x}](\cdot)$ if $\forall t \in \mathbb{R} : \boldsymbol{x}(t) \in [\boldsymbol{x}](t)$.

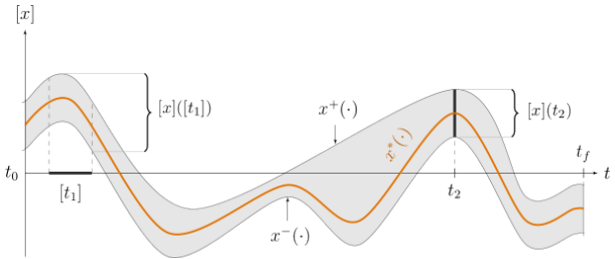

Figure 5: One-dimensional tube enclosing a trajectory $x^*(\cdot)$ plotted in orange. The figure shows two interval evaluations: $[x]([t_1])$ and $[x](t2)$

Evaluation of delay between tubes (Raphael Voges)

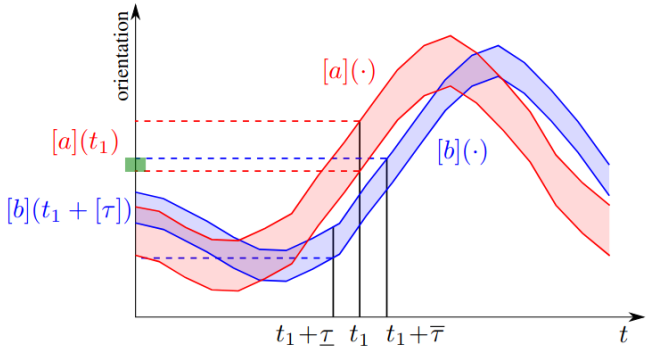

Figure 6: We aim to find the set of all $\tau \in [\tau]$ such that both tubes overlap for every point in time. This requirement is fulfilled for the exemplary $[\tau] = [\underline{\tau}, \overline{\tau}]$ at time t_1 since $[a](t_1)$ and $[b](t_1 + [\tau])$ share a common intersection (green interval).

Offset Constrain Satisfactory Problem (CSP)

The offset Constraint Satisfaction Problem (CSP) is a system of infinite constraints defined as

$$\mathcal{H}_{\text{offset}} : \begin{cases} \textbf{Variables:} & \tau, \boldsymbol{x}(\cdot), \boldsymbol{y}(\cdot) \\ \textbf{Constraints:} & \forall t \in [t] : \boldsymbol{x}(t) = \boldsymbol{y}(t+\tau) \\ \textbf{Domain:} & [\tau], [\boldsymbol{x}](\cdot), [\boldsymbol{y}](\cdot) \end{cases} \tag{1}$$

with the offset domain $[\tau]$ and the tubes domains $[\boldsymbol{x}](\cdot)$ and $[\boldsymbol{y}](\cdot)$ defined on the time interval $[t]$. The offset τ and the trajectories $\boldsymbol{x}(\cdot)$ and $\boldsymbol{y}(\cdot)$ are contained in their respective domain.
The solution set of $\mathcal{H}_{\text{offset}}$ is defined as

$$\mathbb{S}_{\text{offset}} = \{(\tau, \boldsymbol{x}(\cdot), \boldsymbol{y}(\cdot)) \in [\tau] \times [\boldsymbol{x}](\cdot) \times [\boldsymbol{y}](\cdot) \,|\forall t \in [t] : \boldsymbol{x}(t) = \boldsymbol{y}(t+\tau)\}. \tag{2}$$

The contractor of the CSP

The operator

$$\mathcal{C}_{\text{offset}} : \begin{pmatrix} [\tau] \\ [\boldsymbol{x}](\cdot) \\ [\boldsymbol{y}](\cdot) \end{pmatrix} \rightarrow \begin{pmatrix} [\tau'] \\ [\boldsymbol{x}'](\cdot) \\ [\boldsymbol{y}'](\cdot) \end{pmatrix} \tag{3}$$

is a contractor for the CSP $\mathcal{H}_{\text{offset}}$ if it replaces the domains $([\tau], [\boldsymbol{x}](\cdot), [\boldsymbol{y}](\cdot))$ by smaller domains $([\tau'], [\boldsymbol{x}'](\cdot), [\boldsymbol{y}'](\cdot)) \subseteq ([\tau], [\boldsymbol{x}](\cdot), [\boldsymbol{y}](\cdot))$ such that

$$\mathbb{S}_{\text{offset}} \subseteq \left(\left[\tau'\right], \left[\boldsymbol{x}'\right](\cdot), \left[\boldsymbol{y}'\right](\cdot) \right). \tag{4}$$

Theoretical Problem description

Hypothesis : consider the ship trajectory $\boldsymbol{x}(.)$, the land-based estimation tube $[\hat{\boldsymbol{x}}_b](.)$ and the ship-based estimation tube $[\hat{\boldsymbol{x}}_a](.)$. $[\hat{\boldsymbol{x}}_b](.)$ is trustworthy, i.e. $\forall t \in \mathbb{R}, \boldsymbol{x}(t) \in [\hat{\boldsymbol{x}}_b](t)$. $[\hat{\boldsymbol{x}}_a](.)$ has a fault at time t if and only if $\boldsymbol{x}(t) \notin [\hat{\boldsymbol{x}}_a](t)$. Let $\mathcal{D} = \{t \in \mathbb{R} | \boldsymbol{x}(t) \notin [\hat{\boldsymbol{x}}_a](t)\}$ be the set of fault times.

At every time, three hypothesis are considered:

- $\mathcal{H}_0 : \boldsymbol{x}(t) \in [\hat{\boldsymbol{x}}_a](t)$ (no fault)
- $\mathcal{H}_1 : \boldsymbol{x}(t) + \boldsymbol{f}(t) \in [\hat{\boldsymbol{x}}_a](t)$ (value fault with the fault $\boldsymbol{f}(t) \in \mathbb{R}^n$)
- $\mathcal{H}_2 : \boldsymbol{x}(t + \tau) \in [\hat{\boldsymbol{x}}_a](t)$ (delay fault with the delay $\tau \in \mathbb{R}$)

Problem : evaluate $\mathcal{D}$ and the hypothesis $\mathcal{H}_1$ and $\mathcal{H}_2$.

Outline

Fault detection with the overlapping function

The overlapping function is defined by

$$\begin{aligned} o_l : \mathbb{IR}^n \times \mathbb{IR}^n &\to [0,1] \\ ([\boldsymbol{a}], [\boldsymbol{b}]) &\to \frac{\text{Vol}([\boldsymbol{a}] \cap [\boldsymbol{b}])}{\text{Vol}([\boldsymbol{a}])}, \end{aligned} \tag{5}$$

It can invalidate $\mathcal{H}_0$ with the following

$$(o_l([\hat{\boldsymbol{x}}_a](t), [\hat{\boldsymbol{x}}_b](t)) = 0) \Rightarrow t \in \mathcal{D} \text{ (fault)} \tag{6}$$

and one can obtain an inner enclosure of the fault time set

$$\underline{\mathcal{D}} := \{t \in \mathbb{R} | o_l([\hat{\boldsymbol{x}}_a](t), [\hat{\boldsymbol{x}}_b](t)) = 0\}. \tag{7}$$

Evaluation of the fault value with a residual tube

Consider the residual tube $[\boldsymbol{r}](.) = [\hat{\boldsymbol{x}}_a](.) - [\hat{\boldsymbol{x}}_b](.)$. $\forall t \in \mathcal{D}$, consider the fault value $\boldsymbol{f}(t)$ such that $\boldsymbol{x}(t) + \boldsymbol{f}(t) \in [\hat{\boldsymbol{x}}_a](t)$. Then one has

$$\forall t \in \mathcal{D}, \boldsymbol{f}(t) \in [\boldsymbol{r}](t) \tag{8}$$

Delay evaluation

Consider delay CSP

$$\mathcal{H}_{\text{offset}} : \begin{cases} \textbf{Variables:} & \tau, \boldsymbol{x}_a(\cdot), \boldsymbol{x}_b(\cdot) \\ \textbf{Constraints:} & \forall t \in [t] : \boldsymbol{x}_a(t) = \boldsymbol{x}_b(t+\tau) \\ \textbf{Domain:} & [\tau], [\boldsymbol{x}_a](\cdot), [\boldsymbol{x}_b](\cdot) \end{cases} \tag{9}$$

with a contractor $\mathcal{C}_{\text{offset}}$ and an initial delay estimation $[\tau]$. Let

$$\left([\tau'], [\boldsymbol{x}'_a](\cdot), [\boldsymbol{x}'_b](\cdot)\right) = \mathcal{C}_{\text{offset}}\left([\tau], [\boldsymbol{x}_a](\cdot), [\boldsymbol{x}_b](\cdot)\right) \tag{10}$$

Then, one has $\tau \in [\tau']$. Moreover, if $[\tau'] = \emptyset$, then the solution set $\mathbb{S}_{\text{offset}}$ is empty which means that the fault of $[\boldsymbol{x}_a](\cdot)$ cannot be caused by a delay - the hypothesis $\mathcal{H}_2$ is false.

Outline

Method extension to synchronous hybrid systems

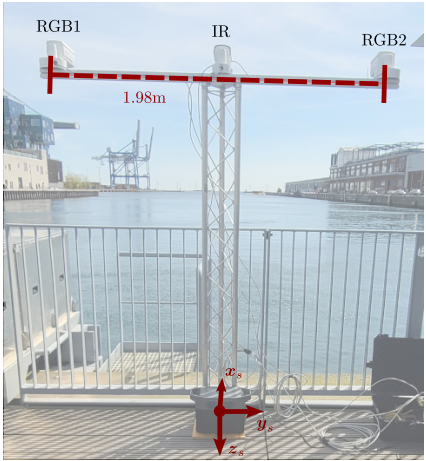

Figure 7: Land-based platform

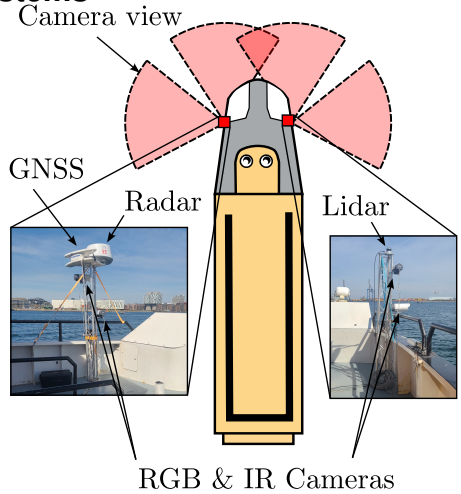

Figure 8: harbour bus

Stereo vision

Images 1 - the ship is close

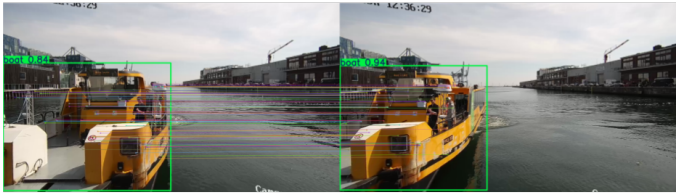

Images 2 - the ship is far

Uncertainty of stereo localisation

The uncertainty of the estimated position $\hat{\boldsymbol{x}}_{\text{stereo}}$ is evaluated with the uncertainty box $[\hat{\boldsymbol{x}}_{\text{stereo}}]$ given by

$$[\hat{\boldsymbol{x}}_{\text{stereo}}] = \begin{bmatrix} \frac{[f]\cdot[b]}{[d]} \\ \left(\frac{[u]-[C_x]}{[d]} + \frac{1}{2}\right)\cdot[b] \end{bmatrix}, \tag{11}$$

with the uncertainty intervals of the centre of the detection box in the left image $\boldsymbol{p} = [u, v] \in \mathbb{Z}^2$, the optical centre of the camera $\boldsymbol{c} = [C_x, C_y] \in \mathbb{Z}^2$, the baseline b, and the focal length f.

Dataset

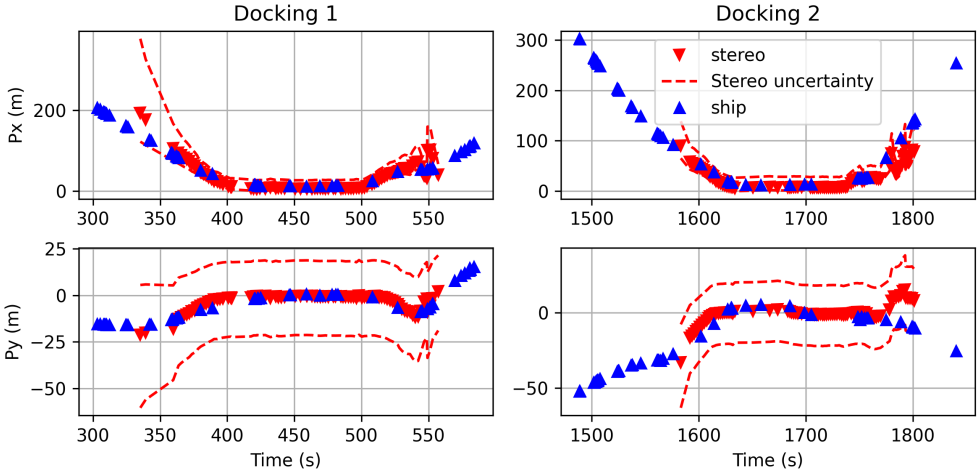
Docking 1
Docking 2
Px (m)
Py (m)
Time (s)
Time (s)
stereo
Stereo uncertainty
ship

Artificial data degradation

3 scenarios are considered:

- **Scenario 0** - no artificial data degradation
- **Scenario 1** - during Docking 1, a value fault starts at time $t_1 = 380$ s with the value

$$\boldsymbol{f}(t) = \begin{bmatrix} 0.5 \text{ m} \cdot (t - t_1) \\ 15 \text{ m} \end{bmatrix}, \tag{12}$$

  added to $[\hat{\boldsymbol{x}}_a](.)$
- **Scenario 2** - during Docking 2, a delay fault start at time $t_2 = 1600$ s with a delay $\tau = 60$ s applied on $[\hat{\boldsymbol{x}}_a](.)$

Outline

Context - Remote pilotage in harbour environment

Tools - Interval analysis

Design of a Fault detection method with tubes

Experimental application

Results

Docking 1 - Scenario 0

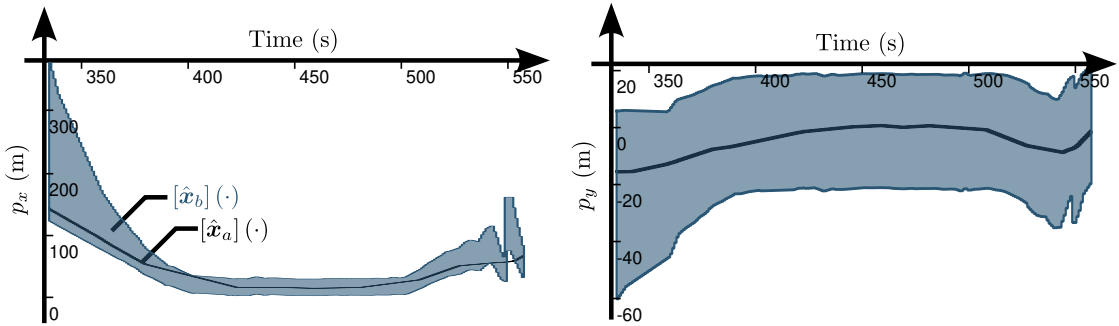

Figure 9: With small exception, there is an intersection between the estimation tubes $[\hat{\boldsymbol{x}}_a]$ (.) from the ship and $[\hat{\boldsymbol{x}}_b]$ (.) the land sensor platform.

Docking 1 - Scenario 1

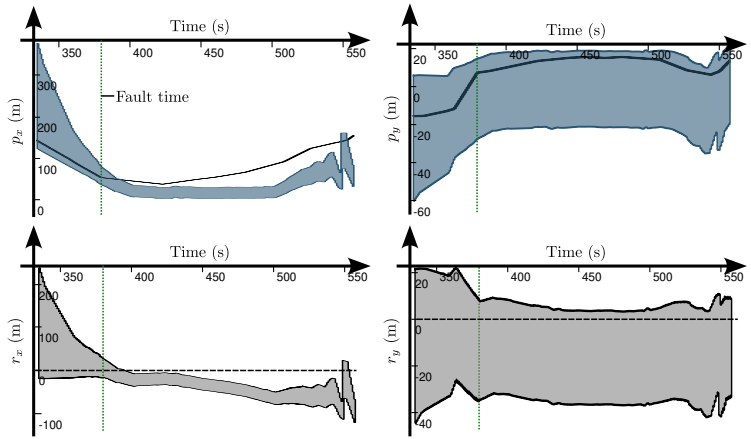

Figure 10: The overlapping function is null on the time intervals $[t_1] = [394, 548]$ and $[t_2] = [553, 557]$. Moreover an empty delay interval $[\tau'] = \emptyset$ is evaluated with $\mathcal{C}_{\text{offset}}$.

Docking 2 - Scenario 0

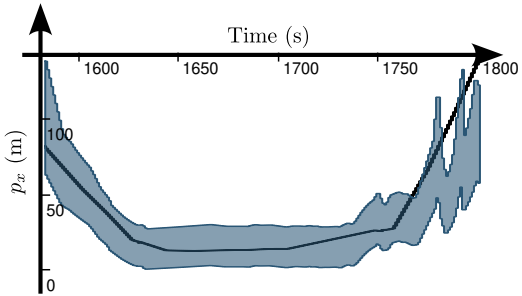

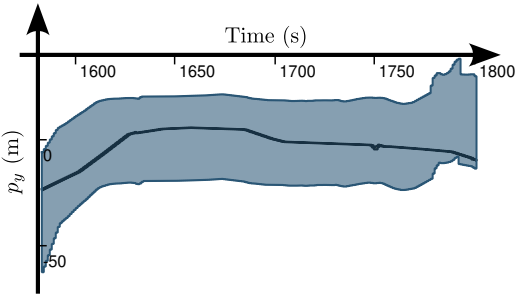

Figure 11: Compared to docking 1, there are more disjoint times when the ship is leaving the docking station ($t > 1750$ s).

Docking 2 - Scenario 2

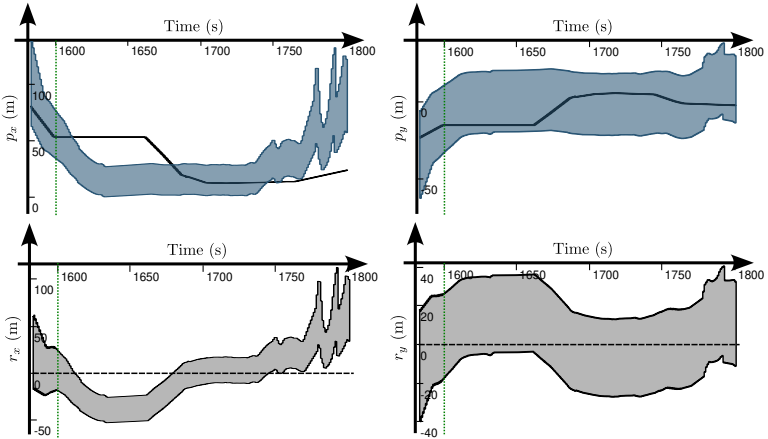

Figure 12: The overlapping function is null on the time intervals $[t_3] = [1611, 1679]$, $[t_4] = [1746, 1752]$ and $[t_5] = [1755, 1801]$. Moreover, the initial delay interval $[\tau] = [0, 100]$, is contracted into $[\tau'] = [52, 77]$

Overlapping function

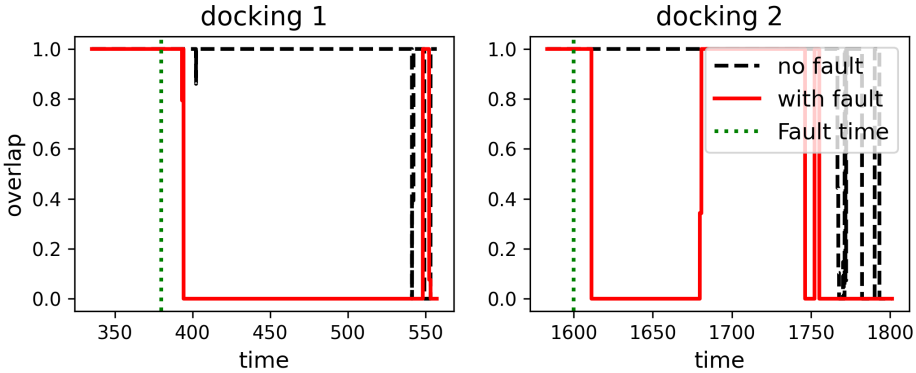

Figure 13: Overlapping function for the different scenarios.

Using Kalman filtering on the stereo tracking

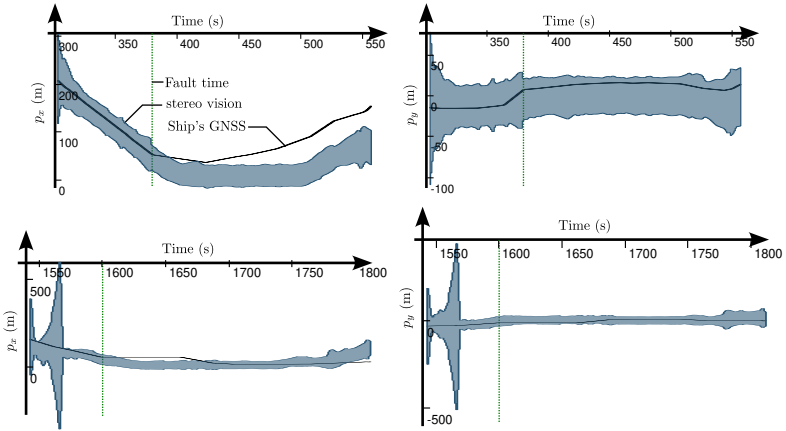

Figure 14: The stereo tubed are obtained via Kalman filtering to remove outliers. Docking 1 is illustrated by the first row, Docking 2 by the second

Kalman filtering - Overlapping function

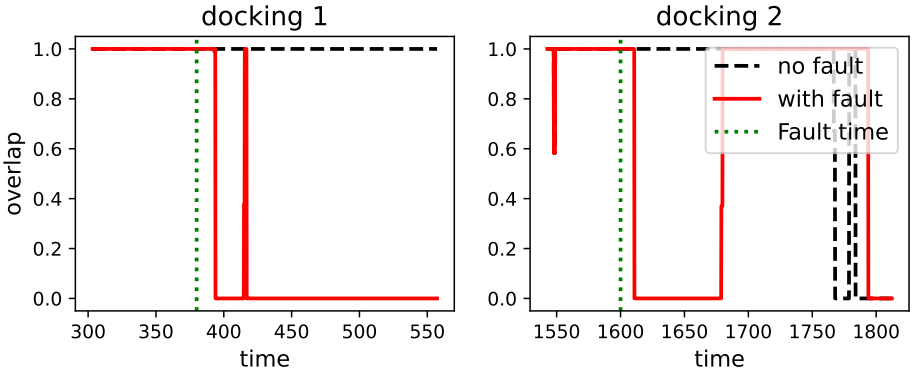

Figure 15: Overlapping function with Kalman filtering.

Conclusion

- The GNSS data faults can be detected with visual localisation. Low Precision sensors can validate high precision measurements.
- Stochastic fault detection methods would have likely given similar results. The tube-based method has less false alarms.
- The camera setup requires an optimisation between the focal length, the field of view and the baseline.
- The results reflect the small data size (<200 samples from each data source).

This work was accepted for the ICMASS Conference 2025.

Future work will broaden data validation to integrate additional sensing modalities, and will explore distributed validation architectures in multi-vessel environments.